HAL open science

High order time discretization for backward semi-Lagrangian methods

Francis Filbet, Charles Prouveur

▶ To cite this version:

Francis Filbet, Charles Prouveur. High order time discretization for backward semi-Lagrangian methods. Journal of Computational and Applied Mathematics, 2016, 303, pp.171-188. hal-01133854

HAL Id: hal-01133854
https://hal.science/hal-01133854v1

Submitted on 20 Mar 2015

HAL is a multi-disciplinary open access archive for the deposit and dissemination of scientific research documents, whether they are published or not. The documents may come from teaching and research institutions in France or abroad, or from public or private research centers.

L'archive ouverte pluridisciplinaire **HAL**, est destinée au dépôt et à la diffusion de documents scientifiques de niveau recherche, publiés ou non, émanant des établissements d'enseignement et de recherche français ou étrangers, des laboratoires publics ou privés.

Public Domain

HIGH ORDER TIME DISCRETIZATION FOR BACKWARD SEMI-LAGRANGIAN METHODS

FRANCIS FILBET, CHARLES PROUVEUR

Abstract. We introduce different high order time discretization schemes for backward semi-Lagrangian methods. These schemes are based on multi-step schemes like Adams-Moulton and Adams-Bashforth schemes combined with backward finite difference schemes. We apply these methods to transport equations for plasma physics applications and for the numerical simulation of instabilities in fluid mechanics. In the context of backward semi-Lagrangian methods, this time discretization strategy is particularly efficient and accurate when the spatial error discretization becomes negligeable and allows to use large time steps.

Keywords. High order time discretization; Semi-Lagrangian scheme; Vlasov-Poisson model; Guiding-centre model; Plasma physics.

Contents

1. Introduction 1
2. The backward semi-Lagrangian method 3
3. High order time discretization for Backward Semi-Lagrangian methods 5
3.1. Second order Adams-Moulton scheme 5
3.2. Third order Adams-Moulton scheme 6
3.3. Third order Adams-Bashforth scheme 7
3.4. Fourth order Adams-Moulton scheme 8
3.5. Fourth order Adams-Bashforth scheme 9
3.6. Milne-Simpson scheme 10
4. Numerical simulations 11
4.1. Test 1 : linear advection 11
4.2. Test 2 : paraxial Vlasov-Poisson model 12
4.3. Test 3 : diocotron instability 14
4.4. Test 4 : Kelvin-Helmoltz instability in a rectangle 16
4.5. Test 5 : shear flow for 2D Euler equations 17
5. Conclusion and perspective 18
References 19

1. Introduction

A model which can be used in many cases for the study of plasma as well as beam propagation is the Vlasov equation coupled with the Maxwell or Poisson equations to compute the self-consistent fields. It describes the evolution of a system of particles under the effects of external and self-consistent fields. The unknown $f(t, \mathbf{x}, \mathbf{v})$, depending on the time t, the position $\mathbf{x}$, and the velocity $\mathbf{v}$, represents the distribution of particles in phase space for each species with $(\mathbf{x}, \mathbf{v}) \in \mathbb{R}^d \times \mathbb{R}^d$, $d = 1, .., 3$. Its behaviour is given by the Vlasov equation,

$$\frac{\partial f}{\partial t} + \mathbf{v} \cdot \nabla_{\mathbf{x}} f + \mathbf{F}(t, \mathbf{x}, \mathbf{v}) \cdot \nabla_{\mathbf{v}} f = 0, \tag{1.1}$$

where the force field $F(t,\mathbf{x},\mathbf{v})$ is coupled with the distribution function f giving a nonlinear system. We first define $\rho(t,\mathbf{x})$ the charge density and $\mathbf{J}(t,\mathbf{x})$ the current density which are given by

$$\rho(t,\mathbf{x}) = q\int_{\mathbb{R}^d} f(t,\mathbf{x},\mathbf{v})d\mathbf{v}, \quad \mathbf{J}(t,\mathbf{x}) = q\int_{\mathbb{R}^d} \mathbf{v}\, f(t,\mathbf{x},\mathbf{v})d\mathbf{v},$$

where q is the elementary charge. For the Vlasov-Poisson model

$$\mathbf{F}(t,\mathbf{x},\mathbf{v}) = \frac{q}{m}\,\mathbf{E}(t,\mathbf{x}), \quad \mathbf{E}(t,\mathbf{x}) = -\nabla_{\mathbf{x}}\phi(t,\mathbf{x}), \quad -\Delta_{\mathbf{x}}\phi = \frac{\rho}{\varepsilon_0}, \tag{1.2}$$

where m represents the mass of one particle. On the other hand for the Vlasov-Maxwell model, we have

$$\mathbf{F}(t,\mathbf{x},\mathbf{v}) = \frac{q}{m}\,(\mathbf{E}(t,\mathbf{x}) + \mathbf{v}\times\mathbf{B}(t,\mathbf{x})\,),$$

and $\mathbf{E}$, $\mathbf{B}$ are solutions of the Maxwell equations

$$\begin{cases} \dfrac{\partial \mathbf{E}}{\partial t} - c^2\nabla\times B = -\dfrac{\mathbf{J}}{\varepsilon_0}, \\[2ex] \dfrac{\partial \mathbf{B}}{\partial t} + \nabla\times\mathbf{E} = 0, \\[2ex] \nabla\cdot\mathbf{E} = \dfrac{\rho}{\varepsilon_0}, \quad \nabla\cdot\mathbf{B} = 0, \end{cases}$$

with the compatibility condition

$$\frac{\partial\rho}{\partial t} + \mathrm{div}_{\mathbf{x}}\mathbf{J} = 0,$$

which is verified by the Vlasov equation solution.

Later on we will also consider the guiding centre model, which has been derived to describe the evolution of the charge density in a highly magnetized plasma in the transverse plane of a tokamak. This model is described as follows: we now consider the density ρ solution to

$$\begin{cases} \dfrac{\partial\rho}{\partial t} + \mathbf{U}\cdot\nabla\rho = 0, \\ -\Delta\phi = \rho, \end{cases} \tag{1.3}$$

where the velocity $\mathbf{U} = (-\partial_y\phi, \partial_x\phi)$ is divergence free.

The numerical resolution of the Vlasov equation and related models is usually performed by Particle-In-Cell (PIC) methods which approximate the plasma by a finite number of particles. Trajectories of these particles are computed from characteristic curves given by the Vlasov equation, whereas self-consistent fields are computed on a mesh of the physical space. This method yields satisfying results with a relatively small number of particles but it is subject to fluctuations, due to the numerical noise, which are difficult to control.

To develop accurate and stable numerical techniques for plasma turbulence, numerical methods based on direct numerical simulation techniques have been developped. The Vlasov equation is discretized in phase space using either semi-Lagrangian [9, 10, 18, 21], finite element [15], finite difference [23] or discontinuous Galerkin [5, 17] schemes.

Among them, the semi-Lagrangian method consists of computing the distribution function at each grid point by following the characteristic curve ending there. Then to compute the value of the distribution function at the origin of the characteristic, a high order interpolation method is needed.

Concerning the time discretization of the backward differential system corresponding to the characteristic curved, it is often performed via a second order splitting scheme, but higher order techniques are also available [1]. This strategy is particulary interesting when each step of the splitting can be explicitly solved. However, it is not always possible to apply a splitting strategy, hence the time discretization technique is often limited to a leap-frog scheme or a

second order predictor-corrector scheme. The aim of the present work is to propose and validate high order techniques to preserve the order of accuracy of the spatial discretization.

This paper is organized as follows : in Section 2 we recall the backward semi-Lagrangian method then in Section 3 we develop different time discretization schemes, based on multi-step methods. Both classical second order schemes and "new" third and fourth order schemes will be proposed. In Section 4, we present several numerical results. In the first, a two-dimensional transport equation with gaussian initial data is investigated to recover the expected order of accuracy. In the second, we perform numerical simulations on the simplified paraxial Vlasov-Poisson model in two dimensions. The last three tests are applied to the guiding centre model to compare the performances of the schemes and to investigate the ability to recover stability results and the development of instabilities.

2. The backward semi-Lagrangian method

To construct a semi-Lagrangian method for (1.1) or (1.3), we consider a generic transport equation written in an advective form

$$\frac{\partial f}{\partial t} + \mathbf{A} \cdot \nabla f = 0, \tag{2.1}$$

where $\mathbf{A} : \mathbb{R}^+ \times \mathbb{R}^d \to \mathbb{R}^d$, $d \geq 1$ and a set of mesh points $(\mathbf{x}_i)_{i \in \mathbb{Z}}$.The main feature of the backward semi-Lagrangian method is to compute an approximated solution to (2.1) by following the characteristics backwards in time

$$\begin{cases} \dfrac{d\mathbf{X}}{dt} = \mathbf{A}, \\ \mathbf{X}(t^{n+1}) = \mathbf{x}_i. \end{cases} \tag{2.2}$$

where $\mathbf{x}_i$ is a mesh point. Thus, we evaluate the distribution function f at this point at time t^{n+1} by following its characteristic curve backward in time until we reach the time when the values of the distribution function f are known, t^n or t^{n-1}. In general the coordinates of the characteristic at this time do not coincide with the mesh points, therefore we need to interpolate the value of the distribution function at this point. Hence, this method can be divided in two steps :

- the first is the resolution of the characteristic differential equation (2.2). This system's solution at time t^n, respectively t^{n-1} depending on the time scheme used, it will be denoted by $\mathbf{X}^n$, respectively $\mathbf{X}^{n-1}$;
- the second step is the interpolation in order to compute an approximation of $f(t^n, \mathbf{X}(t^n))$, since the value of the distribution function is constant along the characteristic, we denote by f^{n+1} the approximation of $f(t^{n+1})$ given by

$$f^{n+1}(\mathbf{x}_i) = \Pi_h f^n(\mathbf{X}^n), \quad i \in \mathbb{Z},$$

  where Π_h is an interpolation operator.

A special case of semi-Lagrangian method for Vlasov-Poisson system, first introduced by Cheng and Knorr [20], is based on a time splitting which enables an exact computation of the characteristics coupled with a cubic spline interpolation for the phase space reconstruction. This algorithm was subsequently applied in many plasma physics papers, see for example [6, 12] and references therein. This method was cast into the more general framework of semi-Lagrangian methods by E. Sonnendrücker *et al.* [21], and successfully adapted to beam physics problems, namely the simulation of space charge waves. For Vlasov type equations, one of the most popular interpolation is the multi-dimensional cubic spline interpolation which is obtained thanks to the tensor product of cubic splines [19]. Another flavor of the semi-Lagrangian method was introduced by Nakamura and Yabe and called the Cubic

Interpolated Propagation (CIP) method. It is based on a Hermite interpolation for which the gradients of the distribution function are also advanced along the characteristics [22]. It needs the storage of f, $\nabla_{\mathbf{x}} f$, and $\nabla_{\mathbf{v}} f$, therefore in order to reduce memory consumption, the mesh on which it is applied should be coarser. We refer to [10, 24] for a comparison of different reconstruction techniques.

Most of these methods based on a time splitting discretization are particularly efficient for classical Vlasov-Poisson or Vlasov-Maxwell systems since the characteristic curves corresponding to the split operator simply become straight lines and can be solved exactly. Therefore, the numerical error is only due to the splitting in time and the phase space discretization of the distribution function. Furthermore for such time splitting schemes, the semi-Lagrangian methods on Cartesian grids coupled with Lagrange, Hermite or cubic spline interpolation techniques are conservative [3, 10].

However, for more elaborated kinetic equations, or even the two dimensional guiding centre model [21], time splitting techniques cannot necessarily be applied. Thus characteristic curves are more sophisticated and require a specific time discretization. For instance, in [13, 14] several numerical solvers have been developed using an Eulerian formulation for gyro-kinetic models. Assume that for all time t^m, $m \leq n$, approximated solutions of the distribution f^m and of the velocity field $\mathbf{A}^m$ are known. The semi-Lagrangian technique based on the leap-frog scheme (2.2) consists in computing $\mathbf{X}^{n-1}$ such that

$$\begin{cases} \dfrac{\mathbf{X}^{n+1} - \mathbf{X}^{n-1}}{2\Delta t} = \mathbf{A}^n(\mathbf{X}^n), \\ \\ \mathbf{X}^{n+1} = \mathbf{x}_i, \end{cases}$$

where the two unknowns $\mathbf{X}^{n-1}$ and $\mathbf{X}^n$ are related by the mid-point rule

$$\frac{\mathbf{X}^{n+1} + \mathbf{X}^{n-1}}{2} = \mathbf{X}^n.$$

Finally, the unknown $\mathbf{X}^{n-1}$ is solution to the following nonlinear problem:

$$\begin{cases} \dfrac{\mathbf{X}^{n+1} - \mathbf{X}^{n-1}}{2\Delta t} = \mathbf{A}^n\left(\dfrac{\mathbf{X}^{n+1} + \mathbf{X}^{n-1}}{2}\right), \\ \mathbf{X}^{n+1} = \mathbf{x}_i. \end{cases} \tag{2.3}$$

However, this scheme is known to generate spurious oscillations in the non-linear phase when small structures occur and it is difficult to distinguish physical and numerical oscillations. Moreover, for these models semi-Lagrangian methods are no more conservative, hence the long time behavior of the numerical solution may become unsuitable.

An alternative time discretization consists in applying a predictor-corrector technique [13, 14]. Assume that at time t^n, approximated solutions of the distribution f^n and of the velocity field $\mathbf{A}^n$ are known. The prediction stage is performed with a half time step : a first order approximation is applied and $\mathbf{X}^n$ is given by

$$\begin{cases} 2\dfrac{\mathbf{X}^{n+\frac{1}{2}} - \mathbf{X}^n}{\Delta t} = \mathbf{A}^n(\mathbf{X}^n), \\ \mathbf{X}^{n+\frac{1}{2}} = \mathbf{x}_i. \end{cases} \tag{2.4}$$

Then we compute the value of the distribution function at time $t^{n+\frac{1}{2}} = t^n + \frac{\Delta t}{2}$ for each mesh point $\mathbf{x}_i$, $i \in \mathbb{Z}$,

$$f^{n+\frac{1}{2}}(\mathbf{x}_i) = \Pi_h f^n(\mathbf{X}^n). \tag{2.5}$$

For nonlinear problems such as (1.1) or (1.3) the velocity field $\mathbf{A}$ depends on f, hence its approximation $\mathbf{A}^{n+1/2}$ at time $t^{n+\frac{1}{2}}$ can be computed from $f^{n+1/2}$. The third stage consists in computing a new approximation of $\mathbf{X}^n$ thanks to the previous prediction and evaluation at time $t^{n+1/2}$ with a second order leap-frog scheme

$$\begin{cases} \dfrac{\mathbf{X}^{n+1}-\mathbf{X}^n}{\Delta t} = \mathbf{A}^{n+\frac{1}{2}}\left(\dfrac{\mathbf{X}^{n+1}+\mathbf{X}^n}{2}\right), \\ \mathbf{X}^{n+\frac{1}{2}} = \mathbf{x}_i. \end{cases} \tag{2.6}$$

Finally, for the fourth stage, the value of the solution is given by a last interpolation :

$$f^{n+1}(\mathbf{x}_i) \;=\; \Pi_h\, f^n(\mathbf{X}^n). \tag{2.7}$$

This method gives much more stable and accurate results than the previous leap-frog scheme (2.3), but it requires one more interpolation and thus has a higher computational cost compared to other methods of the same order of precision. Furthermore, it is limited to second order accuracy whereas the interpolation procedure commonly based on cubic spline techniques of high degree interpolations is third order accurate.

For this purpose, we want to develop a class of high order numerical schemes specifically designed for backward semi-Lagrangian method. In the following we present several schemes based on Adams-Moulton and Adams-Bashforth time discretization techniques applied in the framework of backward semi-Lagrangian methods.

3. High order time discretization for Backward Semi-Lagrangian methods

In this section, we fix a time step $\Delta t > 0$ and assume that the velocity field $\mathbf{A}^m$ and the distribution function f^m have been approximated for all time step $t^m = m\,\Delta t$, $m \le n$, we look for an approximation $\mathbf{X}^n$ of the solution the system (2.2) at time t^n.

Hence, we will construct different high order scheme in the following form

$$\mathbf{X}^n = \mathbf{x}_i - \Delta t\,\Phi(\Delta t, t^{n+1}, \mathbf{x}_i), \tag{3.8}$$

where Φ also depends on $\mathbf{A}$ at different times. This framework allows to study consistency and stability of the different numerical schemes using a systematic way. Indeed, for the consistency analysis we have [16]

Proposition 3.1. *Assume that the velocity field $\boldsymbol{A}$ is given. The scheme (3.8) is consistent if we have $\Phi(0, t^{n+1}, \mathbf{x}_i) = \boldsymbol{A}(t^{n+1}, \mathbf{x}_i)$. Moreover, the scheme is consistent of order p if*

$$\frac{\partial^k \Phi}{\partial s^k}(s=0, t^{n+1}, \mathbf{x}_i) = \frac{(-1)^{k+1}}{k+1}\boldsymbol{A}^{(k)}(t^{n+1}, \mathbf{x}_i), \quad 0 \le k \le p,$$

where $\boldsymbol{A}^{(0)} = \boldsymbol{A}$ and for $k \ge 1$

$$\boldsymbol{A}^{(k)} = \frac{\partial}{\partial t}\boldsymbol{A}^{(k-1)} + \boldsymbol{A}\cdot\nabla_{\mathbf{x}}\boldsymbol{A}^{(k-1)}.$$

3.1. Second order Adams-Moulton scheme.

We first consider the implicit Adams-Moulton scheme, which is second order accurate :

$$\frac{\mathbf{X}^{n+1}-\mathbf{X}^n}{\Delta t} = \frac{1}{2}\,(\mathbf{A}^{n+1}(\mathbf{X}^{n+1}) + \mathbf{A}^n(\mathbf{X}^n)).$$

Unfortunately, the velocity field $\mathbf{A}$ is not known at time $(t^{n+1}$, thus a high order reconstruction is performed using an affine extrapolation in time using previous time steps t^{n-1} and t^n, it yields

$$\mathbf{A}^{n+1}(\mathbf{X}^{n+1}) \;=\; 2\,\mathbf{A}^n(\mathbf{X}^{n+1}) - \mathbf{A}^{n-1}(\mathbf{X}^{n+1}).$$

Therefore the approximation $\mathbf{X}^n$ is found by solving:

$$\begin{cases} \dfrac{\mathbf{X}^{n+1}-\mathbf{X}^n}{\Delta t} = \dfrac{1}{2}\ \big(2\,\mathbf{A}^n(\mathbf{X}^{n+1}) - \mathbf{A}^{n-1}(\mathbf{X}^{n+1}) + \mathbf{A}^n(\mathbf{X}^n)\big), \\ \mathbf{X}^{n+1} = \mathbf{x}_i. \end{cases} \tag{3.9}$$

This nonlinear system can be either solved using a classical fixed point or Newton method or approximated by a linear system using a piecewise affine approximation of $\mathbf{A}^n$.

It can be written in the form

$$\mathbf{X}^n = \mathbf{x}_i - \Delta t\,\Phi(\Delta t, t^{n+1}, \mathbf{x}_i),$$

where the function Φ is implicitly defined.

Proposition 3.2. *Assume that the velocity field $\boldsymbol{A} \in \mathcal{C}^1(\mathbb{R}^+ \times \mathbb{R}^d)$ is given. The scheme (3.9) is consistent and second order accurate.*

Proof. Assume that $\mathbf{A}$ is given and $\mathbf{A} \in \mathcal{C}^1$. From the definition of the second order Adams-Moulton scheme (3.9), we define implicitly Φ such that

$$\begin{aligned} \Phi(\Delta t, t^{n+1}, \mathbf{x}_i) \;=\; & \frac{1}{2}\big[2\mathbf{A}(t^{n+1}-\Delta t, \mathbf{x}_i) - \mathbf{A}(t^{n+1}-2\Delta t, \mathbf{x}_i) \\ & + \mathbf{A}\left(t^{n+1}-\Delta t, \mathbf{x}_i - \Delta t\ \Phi(t^{n+1}, \mathbf{x}_i, \Delta t)\right)\ \big]. \end{aligned}$$

Therefore, we easily verify that $\Phi(0, t^{n+1}, \mathbf{x}_i) = \mathbf{A}(t^{n+1}, \mathbf{x}_i)$ anf furthermore by differentiating with respect to Δt, we get that

$$\frac{\partial \Phi}{\partial s}(s=0, t^{n+1}, \mathbf{x}_i) = -\frac{1}{2}\left[\frac{\partial \mathbf{A}}{\partial t} + \mathbf{A}\cdot\nabla_{\mathbf{x}}\mathbf{A}\right](t^{n+1}, \mathbf{x}_i).$$

Hence the scheme is second order accurate. □

3.2. **Third order Adams-Moulton scheme.** Now we start from the third order accurate Adams-Moulton scheme applied to (2.2), it gives

$$\frac{\mathbf{X}^{n+1}-\mathbf{X}^n}{\Delta t} = \frac{1}{12}\ \big(5\ \mathbf{A}^{n+1}(\mathbf{X}^{n+1}) + 8\ \mathbf{A}^n(\mathbf{X}^n) - \mathbf{A}^{n-1}(\mathbf{X}^{n-1})\big)\,.$$

In order to define rigourously the numerical approximation $\mathbf{X}^n$ we need to fix two different issues. The first one is to obtain an approximation $\mathbf{A}^{n+1}$ of the velocity field $\mathbf{A}$ at time t^{n+1}, which preserves the order of accuracy up to third order. Therefore, as for the previous scheme, we extrapolate the velocity field $\mathbf{A}$ from the values at the previous time steps using a Lagrange interpolation polynomial of degree two, that is,

$$\mathbf{A}^{n+1}(\mathbf{X}^{n+1}) \;=\; 3\ \mathbf{A}^n(\mathbf{X}^{n+1}) - 3\ \mathbf{A}^{n-1}(\mathbf{X}^{n+1}) + \mathbf{A}^{n-2}(\mathbf{X}^{n+1}).$$

The second issue we have to address, comes from the fact that the third order Adams-Moulton scheme is a two steps scheme *i.e.* we have introduced an additional unknown $\mathbf{X}^{n-1}$. Hence, another relation between the unknowns $\mathbf{X}^{n-1}$ and $\mathbf{X}^n$ is needed and, as for the previous extrapolation, it has to preserve the order of accuracy of the scheme. Let us consider the following polynomial $\mathbf{P}_2(t)$ such that

$$\begin{cases} \mathbf{P}_2(t^{n+1}) = \mathbf{X}^{n+1}, \\ \mathbf{P}_2(t^n) = \mathbf{X}^n, \\ \dfrac{d\mathbf{P}_2}{dt}(t^{n+1}) = \mathbf{A}^{n+1}(\mathbf{X}^{n+1}), \end{cases}$$

where the velocity field $\mathbf{A}^{n+1}$ has been computed using the previous extrapolation step. Finally, we define $\mathbf{X}^{n-1} = \mathbf{P}_2(t^{n-1})$, which yields the following relation

$$\mathbf{X}^{n-1} \;=\; 4\mathbf{X}^n - 3\;\mathbf{X}^{n+1} + 2\;\Delta t\;\mathbf{A}^{n+1}.$$

Gathering the previous approximations, it gives the following one step scheme

$$\begin{cases} \dfrac{\mathbf{X}^{n+1}-\mathbf{X}^n}{\Delta t} = \dfrac{1}{12}\;\left(5\;\mathbf{A}^{n+1}(\mathbf{X}^{n+1}) \;+\; 8\mathbf{A}^n(\mathbf{X}^n) - \mathbf{A}^{n-1}(\mathbf{X}^{n-1})\right), \\ \mathbf{A}^{n+1}(\mathbf{X}^{n+1}) \;=\; 3\;\mathbf{A}^n(\mathbf{X}^{n+1}) - 3\;\mathbf{A}^{n-1}(\mathbf{X}^{n+1}) + \mathbf{A}^{n-2}(\mathbf{X}^{n+1}), \\ \mathbf{X}^{n-1} = 4\;\mathbf{X}^n - 3\;\mathbf{X}^{n+1} + 2\;\Delta t\mathbf{A}^{n+1}(\mathbf{X}^{n+1}), \\ \mathbf{X}^{n+1} = \mathbf{x}_i. \end{cases} \tag{3.10}$$

It can be written in the form

$$\mathbf{X}^n = \mathbf{x}_i - \Delta t\,\Phi(\Delta t, t^{n+1}, \mathbf{x}_i),$$

where the function Φ is implicitly defined. By following the lines of Proposition 3.2 and after some calculus we show that

Proposition 3.3. *Assume that the velocity field $\boldsymbol{A} \in \mathcal{C}^2(\mathbb{R}^+ \times \mathbb{R}^d)$ is given. The scheme (3.10) is consistent and third order accurate.*

Proof. Assume that $\mathbf{A}$ is given and $\mathbf{A} \in \mathcal{C}^1$. We first construct an approximation of $\mathbf{A}$ at time t^{n+1} as a function of Δt, that is,

$$\mathbf{A}^{n+1}(\Delta t) \;=\; 3\;\mathbf{A}(t^{n+1}-\Delta t) - 3\;\mathbf{A}(t^{n+1}-2\Delta t) \;+\; \mathbf{A}(t^{n+1}-3\Delta t).$$

From the definition of the third order Adams-Moulton scheme (3.10), we define implicitly Φ such that

$$\begin{aligned} \Phi(\Delta t, t^{n+1}, \mathbf{x}_i) \;&=\; \frac{1}{12}\left[5\mathbf{A}^{n+1}(\Delta t, \mathbf{x}_i) + 8\,\mathbf{A}\left(t^{n+1}-\Delta t, \mathbf{x}_i - \Delta t\;\Phi(\Delta t, t^{n+1}, \mathbf{x}_i)\right)\right. \\ &-\; \left.\mathbf{A}\left(t^{n+1}-2\Delta t, \mathbf{x}_i - 4\Delta t\;\Phi(\Delta t, t^{n+1}, \mathbf{x}_i) \;+\; 2\,\Delta t\,\mathbf{A}^{n+1}(\Delta t, \mathbf{x}_i)\right)\right]. \end{aligned}$$

Therefore, we easily verify that $\Phi(0, t^{n+1}, \mathbf{x}_i) = \mathbf{A}(t^{n+1}, \mathbf{x}_i)$ anf furthermore by differentiating with respect to Δt, we get that

$$\frac{\partial \Phi}{\partial s}(s=0, t^{n+1}, \mathbf{x}_i) = \left[\frac{\partial \mathbf{A}}{\partial t} + \mathbf{A}\cdot\nabla_{\mathbf{x}}\mathbf{A}\right](t^{n+1}, \mathbf{x}_i),$$

which proves that the scheme is second order accurate. Finally, to show that (3.10) is third order, we compute

$$\begin{aligned} \frac{\partial^2 \Phi}{\partial s^2}(s=0, t^{n+1}, \mathbf{x}_i) \;&=\; \frac{1}{3}\left(\frac{\partial^2 \mathbf{A}}{\partial s^2} + 2\,\frac{\partial}{\partial s}\nabla_{\mathbf{x}}\mathbf{A} + \mathbf{A}^{(1)}\nabla_{\mathbf{x}}\mathbf{A} + \mathbf{A}\cdot\nabla^2_{\mathbf{x}}\mathbf{A}\cdot\mathbf{A}\right), \\ &=\; \frac{1}{3}\mathbf{A}^2(t^{n+1}, \mathbf{x}_i). \end{aligned}$$

□

3.3. **Third order Adams-Bashforth scheme.** We now start from the third order explicit Adams scheme applied to 2.2, it first gives that

$$\frac{\mathbf{X}^{n+1}-\mathbf{X}^n}{\Delta t} = \frac{1}{12}\left(23\;\mathbf{A}^n(\mathbf{X}^n) - 16\;\mathbf{A}^{n-1}(\mathbf{X}^{n-1}) + 5\;\mathbf{A}^{n-2}(\mathbf{X}^{n-2})\right).$$

The stencil here is different from the previous one for the Adams-Moulton scheme since we do not need to compute an approximation for $\mathbf{A}^{n+1}$, we use a slightly different polynomial to approximate $\mathbf{X}^{n-1}$ and $\mathbf{X}^{n-2}$.

The main issue comes now from the fact that the third order Adams scheme is a three steps scheme *i.e.* we have introduced additional unknowns $\mathbf{X}^{n-2}$ and $\mathbf{X}^{n-1}$. To compute them, let us consider the following polynomial $\mathbf{P}_2(t)$ such that

$$\begin{cases} \mathbf{P}_2(t^{n+1}) = \mathbf{X}^{n+1}, \\ \mathbf{P}_2(t^n) = \mathbf{X}^n, \\ \dfrac{d\mathbf{P}_2}{dt}(t^n) = \mathbf{A}^n(\mathbf{X}^n). \end{cases}$$

We set $\mathbf{X}^n = \mathbf{x}_i - \mathbf{c}_n$ and from the polynomial $\mathbf{P}_2$, we can define $\mathbf{X}^{n-1}$ and $\mathbf{X}^{n-2}$ by

$$\begin{cases} \mathbf{X}^{n-1} = \mathbf{x}_i - 2\ \Delta t\ \mathbf{A}^n(\mathbf{X}^n), \\ \mathbf{X}^{n-2} = \mathbf{x}_i + 3\ \mathbf{c}_n - 6\ \Delta t\ \mathbf{A}^n(\mathbf{X}^n). \end{cases}$$

Gathering these approximations, it leads to the resolution of a nonlinear problem which is again solved with a Newton algorithm:

$$\begin{cases} \dfrac{\mathbf{X}^{n+1} - \mathbf{X}^n}{\Delta t} = \dfrac{1}{24}\left(23\ \mathbf{A}^n(\mathbf{X}^n) - 16\ \mathbf{A}^{n-1}(\mathbf{X}^{n-1}) + 5\ \mathbf{A}^{n-2}(\mathbf{X}^{n-2})\right), \\ \mathbf{X}^{n-2} = \mathbf{x}_i + 3\ \mathbf{c}_n - 6\ \Delta t\ \mathbf{A}^n(\mathbf{X}^n), \\ \mathbf{X}^{n-1} = \mathbf{x}_i - 2\ \Delta t\ \mathbf{A}^n(\mathbf{X}^n), \\ \mathbf{X}^n = \mathbf{x}_i - \mathbf{c}_n, \\ \mathbf{X}^{n+1} = \mathbf{x}_i. \end{cases} \tag{3.11}$$

Let us note that this scheme requires more memory since it needs the storage of the last three time steps of the velocity field. It is also slightly more complicated than the implicit scheme of the same order.

By following the lines of Proposition 3.3 and after some calculus we show that

Proposition 3.4. *Assume that the velocity field $\boldsymbol{A} \in \mathcal{C}^2(\mathbb{R}^+ \times \mathbb{R}^d)$ is given. The scheme (3.11) is consistent and third order accurate.*

3.4. **Fourth order Adams-Moulton scheme.** We first consider the fourth order Adams-Moulton scheme:

$$\frac{\mathbf{X}^{n+1} - \mathbf{X}^n}{\Delta t} = \frac{1}{24}\left(9\ \mathbf{A}^{n+1}(\mathbf{X}^{n+1}) + 19\ \mathbf{A}^n(\mathbf{X}^n) - 5\ \mathbf{A}^{n-1}(\mathbf{X}^{n-1}) + \mathbf{A}^{n-2}(\mathbf{X}^{n-2})\right).$$

The stencil is now quite large and we need an approximation of $\mathbf{A}^{n+1}$ of order $O(\Delta t^4)$. Therefore we take:

$$\mathbf{A}^{n+1}(\mathbf{x}) = 4\ \mathbf{A}^n(\mathbf{x}) - 6\ \mathbf{A}^{n-1}(\mathbf{x}) + 4\ \mathbf{A}^{n-2}(\mathbf{x}) - \mathbf{A}^{n-3}(\mathbf{x}).$$

To complete the numerical approximation, new relations are needed for $\mathbf{X}^{n-1}$ and $\mathbf{X}^{n-2}$. To this aim, we consider the following cubic Hermite interpolation polynomial $\mathbf{P}_3(t)$ such that

$$\begin{cases} \mathbf{P}_3(t^{n+1}) = \mathbf{X}^{n+1}, \\ \mathbf{P}_3(t^n) = \mathbf{X}^{n+1}, \\ \dfrac{d\mathbf{P}_3}{dt}(t^n) = \mathbf{A}^n(\mathbf{X}^n), \\ \dfrac{d\mathbf{P}_3}{dt}(t^{n+1}) = \mathbf{A}^{n+1}(\mathbf{X}^{n+1}), \end{cases}$$

where the velocity field $\mathbf{A}^{n+1}$ has been computed using the previous extrapolation step.

Thus we set $\mathbf{X}^n = \mathbf{x}_i - \mathbf{c}_n$ and $\mathbf{X}^{n+1} = \mathbf{x}_i$, and obtain

$$\begin{cases} \mathbf{X}^{n-1} = \mathbf{x}_i + 4\mathbf{c}_n - 2\Delta t \left(2\mathbf{A}^n(\mathbf{X}^n) + \mathbf{A}^{n+1}(\mathbf{X}^{n+1}) \right), \\ \mathbf{X}^{n-2} = \mathbf{x}_i + 9\mathbf{c}_n - 3\Delta t \left(3\mathbf{A}^n(\mathbf{X}^n) + \mathbf{A}^{n+1}(\mathbf{X}^{n+1}) \right). \end{cases}$$

Gathering the previous approximations, it gives the following one step scheme

$$\begin{cases} \dfrac{\mathbf{X}^{n+1} - \mathbf{X}^n}{\Delta t} = \\ \qquad \dfrac{1}{24} \left(9\mathbf{A}(\mathbf{X}^{n+1}) + 19\mathbf{A}^n(\mathbf{X}^n) - 5\mathbf{A}^{n-1}(\mathbf{X}^{n-1}) + \mathbf{A}^{n-2}(\mathbf{X}^{n-2}) \right), \\ \mathbf{A}^{n+1}(\mathbf{X}^{n+1}) = \\ \qquad 4\ \mathbf{A}^n(\mathbf{X}^{n+1}) - 6\ \mathbf{A}^{n-1}(\mathbf{X}^{n+1}) + 4\ \mathbf{A}^{n-2}(\mathbf{X}^{n+1}) - \mathbf{A}^{n-3}(\mathbf{X}^{n+1}), \\ \mathbf{X}^{n-2} = \mathbf{x}_i + 27\mathbf{c}_n - 6\Delta t \left(3\mathbf{A}^n(\mathbf{X}^n) + 2\mathbf{A}^{n+1}(\mathbf{X}^{n+1}) \right), \\ \mathbf{X}^{n-1} = \mathbf{x}_i + 4\mathbf{c}_n - 2\Delta t \left(2\mathbf{A}^n(\mathbf{X}^n) + \mathbf{A}^{n+1}(\mathbf{X}^{n+1}) \right), \\ \mathbf{X}^n = \mathbf{x}_i - \mathbf{c}_n, \\ \mathbf{X}^{n+1} = \mathbf{x}_i. \end{cases} \tag{3.12}$$

which can be solved through fixed point iteration procedure.

By following the lines of Proposition 3.3 and after some heavy calculus we show that

Proposition 3.5. *Assume that the velocity field $\boldsymbol{A} \in \mathcal{C}^3(\mathbb{R}^+ \times \mathbb{R}^d)$ is given. The scheme (3.12) is consistent and fourth order accurate.*

3.5. **Fourth order Adams-Bashforth scheme.** We now start from the fourth order explicit Adams scheme applied to 2.2, it first gives that

$$\frac{\mathbf{X}^{n+1} - \mathbf{X}^n}{\Delta t} = \frac{1}{24} \left(55\ \mathbf{A}^n(\mathbf{X}^n) - 59\ \mathbf{A}^{n-1}(\mathbf{X}^{n-1}) + 37\ \mathbf{A}^{n-2}(\mathbf{X}^{n-2}) - 9\ \mathbf{A}^{n-3}(\mathbf{X}^{n-3}) \right).$$

The stencil here is different from the previous one for the Adams-Moulton scheme since we do not need to compute an approximation for $\mathbf{A}^{n+1}$, we use a slightly different polynomial to approximate $\mathbf{X}^{n-1}$, $\mathbf{X}^{n-2}$ and $\mathbf{X}^{n-3}$.

The main issue comes now from the fact that the fourth order Adams scheme is a four steps scheme *i.e.* we have introduced additional unknowns $\mathbf{X}^{n-3}$, $\mathbf{X}^{n-2}$ and $\mathbf{X}^{n-1}$. To compute them, let us consider the following polynomial $\mathbf{P}_3(t)$ such that

$$\begin{cases} \mathbf{P}_3(t^{n+1}) = \mathbf{X}^{n+1}, \\ \mathbf{P}_3(t^n) = \mathbf{X}^n, \\ \dfrac{d\mathbf{P}_3}{dt}(t^n) = \mathbf{A}^n(\mathbf{X}^n), \\ \dfrac{d\mathbf{P}_3}{dt}(t^{n-1}) = \mathbf{A}^{n-1}(\mathbf{X}^{n-1}). \end{cases}$$

We set $\mathbf{X}^n = \mathbf{x}_i - \mathbf{c}_n$ and from the polynomial $\mathbf{P}_3$, we can define $\mathbf{X}^{n-1}$, $\mathbf{X}^{n-2}$ and $\mathbf{X}^{n-3}$ by

$$\begin{cases} \mathbf{X}^{n-1} = \mathbf{x}_i - 2\ \Delta t\ \mathbf{A}^n(\mathbf{X}^n), \\ \mathbf{X}^{n-2} = \mathbf{x}_i - 3\ \mathbf{c}_n + 3\ \Delta t\ \left(\ \mathbf{A}^n(\mathbf{X}^n) - \mathbf{A}^{n-1}(\mathbf{X}^{n-1})\ \right), \\ \mathbf{X}^{n-3} = \mathbf{x}_i - 16\ \mathbf{c}_n + 12\ \Delta t\ \left(\ 2\ \mathbf{A}^n(\mathbf{X}^n) - \mathbf{A}^{n-1}(\mathbf{X}^{n-1})\ \right).. \end{cases}$$

Gathering these approximations, it leads to the resolution of a nonlinear problem which is again solved with a Newton algorithm:

$$\begin{cases} \dfrac{\mathbf{X}^{n+1} - \mathbf{X}^n}{\Delta t} = \\ \qquad \dfrac{1}{24}\left(55\ \mathbf{A}^n(\mathbf{X}^n) - 59\ \mathbf{A}^{n-1}(\mathbf{X}^{n-1}) + 37\ \mathbf{A}^{n-2}(\mathbf{X}^{n-2}) - 9\ \mathbf{A}^{n-3}(\mathbf{X}^{n-3})\right), \\ \mathbf{X}^{n-3} = \mathbf{x}_i - 16\ \mathbf{c}_n + 12\ \Delta t\ \left(\ 2\ \mathbf{A}^n(\mathbf{X}^n) - \mathbf{A}^{n-1}(\mathbf{X}^{n-1})\ \right), \\ \mathbf{X}^{n-2} = \mathbf{x}_i - 3\ \mathbf{c}_n + 3\ \Delta t\ \left(\ \mathbf{A}^n(\mathbf{X}^n) - \mathbf{A}^{n-1}(\mathbf{X}^{n-1})\ \right), \\ \mathbf{X}^{n-1} = \mathbf{x}_i - 2\ \Delta t\ \mathbf{A}^n(\mathbf{X}^n), \\ \mathbf{X}^n = \mathbf{x}_i - \mathbf{c}_n, \\ \mathbf{X}^{n+1} = \mathbf{x}_i. \end{cases} \tag{3.13}$$

Let us note that this scheme requires more memory since it needs the storage of the last four time steps of the velocity field. It is also slightly more complicated than the implicit scheme of the same order.

By following the lines of Proposition 3.3 and after some heavy calculus we show that

Proposition 3.6. *Assume that the velocity field $\boldsymbol{A} \in \mathcal{C}^3(\mathbb{R}^+ \times \mathbb{R}^d)$ is given. The scheme (3.13) is consistent and fourth order accurate.*

3.6. **Milne-Simpson scheme.** The last scheme we want to investigate is based on the two steps fourth order Milne-Simpson scheme given by

$$\frac{\mathbf{X}^{n+1} - \mathbf{X}^{n-1}}{2\Delta t} = \frac{1}{6}\ (\mathbf{A}^{n+1} + 4\ \mathbf{A}^n + \mathbf{A}^{n-1}).$$

We proceed as for the implicit third order Adams scheme, and obtain the following two steps scheme

$$
\begin{cases}
\dfrac{\mathbf{X}^{n+1}-\mathbf{X}^{n-1}}{2\Delta t} = \dfrac{1}{6}\,(\mathbf{A}^{n+1}+4\,\mathbf{A}^{n}+\mathbf{A}^{n-1}).,\\
\mathbf{A}^{n+1}(\mathbf{X}^{n+1}) = 4\,\mathbf{A}^{n}(\mathbf{X}^{n+1}) - 6\,\mathbf{A}^{n-1}(\mathbf{X}^{n+1}) + 4\,\mathbf{A}^{n-2}(\mathbf{X}^{n+1}) - \mathbf{A}^{n-3}(\mathbf{X}^{n+1}),\\
\mathbf{X}^{n-1} = \mathbf{x}_i + 4\mathbf{c}_n - 2\Delta t\left(2\mathbf{A}^{n}(\mathbf{X}^{n}) + \mathbf{A}^{n+1}(\mathbf{X}^{n+1})\right),\\
\mathbf{X}^{n} = \mathbf{x}_i - \mathbf{c}_n,\\
\mathbf{X}^{n+1} = \mathbf{x}_i.
\end{cases}
\tag{3.14}
$$

This scheme is not a one step scheme and does not enter in the class presented at the beginning.

4. Numerical simulations

In this section we will compare the different time discretization for the backward semi-Lagrangian method using the classical cubic spline interpolation and also the fifth order Hermite interpolation. Reference solutions will be computed using a fifth order finite difference technique with a WENO reconstruction coupled with a fourth order Runge-Kutta scheme for the time discretization with a small time step [24]. The first numerical test concerns a simple linear advection problem for which we can compute an exact solution and verify the order of accuracy. The next simulations concern the development of instabilities for the paraxial Vlasov-Poisson approximation and the guiding centre model.

4.1. **Test 1 : linear advection.** We first consider a linear advection problem given by

$$
\begin{cases}
\dfrac{\partial f}{\partial t} + \mathbf{V}\cdot\nabla_{\mathbf{x}} f = 0, \quad \mathbf{x}\in\mathbb{R}^2,\, t>0,\\
f(0,\mathbf{x}) = e^{-\|\mathbf{x}\|^2},
\end{cases}
$$

where $\mathbf{V}(t,\mathbf{x}) = \tan(t)\,\mathbf{x}/2$. For this equation, we can compute an exact solution, it yields

$$
f(t,\mathbf{x}) = e^{-\|\mathbf{x}\|^2\,\cos(t)}.
$$

We define the discrete L^2 norm of the error as;

$$
\varepsilon_2 = \max_{0\le n\le N_t}\left(\sum_{\mathbf{i}} h^2\,\|f^n_{\mathbf{i}} - f(t^n,\mathbf{x_i})\|^2\right)^{1/2}.
$$

On the one hand, the computational domain is reduced to the square $[-6,6]^2$ and we introduce the grid size $h = 1/N_{\mathbf{x}}$ such that the grid point are given by $\mathbf{x_i} = \mathbf{i}\,h$ where $\mathbf{i}\in\mathbb{Z}^2$. On the other hand, for the time discretization, we choose the time step $\Delta t = 1/N_t$ and $t^n = n\Delta t$, with $n\in\mathbb{N}$. Therefore, the mesh can be described only by the couple $(N_t, N_{\mathbf{x}})$. To estimate the order of accuracy of the schemes we compute a numerical approximation and refine the time step Δt according to the space step h in such a way the CFL condition associated to the advection equation is equal to 2.

Absolute error in discrete L^2 norms at time $T=1$ are shown in Table 1 for all the schemes presented in the previous section. In order to focus on the time discretization error, a large time step is used with a fine grid for the spatial discretization. As expected the order of accuracy is satisfied for all second, third and fourth order schemes.

Furthermore, in Table 2 we indicate the computational time for each discretization . We notice that the Adams-Moulton schemes are actually faster than the Adams-Bashforth schemes and much more precise. On the other hand, the second order Adams-Moulton is faster than

$(N_t, N_{\mathbf{x}})$	(40,200)		(80,400)		(160,800)	
	$\|\cdot\|_2$	r	$\|\cdot\|_2$	r	$\|\cdot\|_2$	r
Second order Predictor - Corrector (2.4)	4.6e-4	1.97	1.14e-4	2.0	2.86e-5	2.0
Second order Adams-Moulton (3.9)	4.8e-3	1.91	1.2e-3	2.0	3.0e-4	2.0
Third order Adams-Moulton (3.10)	2.77e-4	2.80	3.7-5	2.90	4.8e-6	2.94
Third order Adams-Bashforth (3.11)	5.72e-4	2.78	7.7e-5	2.89	1.0e-5	2.94
Fourth order Adams-Moulton (3.12)	2.99e-5	3.62	2.14e-6	3.80	1.44e-7	3.89
Fourth order Adams-Bashforth (3.13)	6.92e-5	3.62	4.96e-6	3.80	3.33e-7	3.90
Fourth order Milne-Simpson (3.14)	1.63e-5	3.71	1.12e-6	3.86	7.37e-8	3.93

TABLE 1. Comparison of different time discretization schemes for the backward semi-Lagrangian method : error L^2-norm and order of convergence r. The final time is $T = 1$.

$(N_t, N_{\mathbf{x}})$	(20,100)	(40,200)	(80,400)	(160,800)
Second order Predictor - Corrector (2.4)	0.27	2.0	16.9	135
Second order Adams-Moulton (3.9)	0.16	1.08	9.24	67.3
Third order Adams-Moulton (3.10)	0.6	4.4	31.5	228
Third order Adams-Bashforth (3.11)	0.74	5.6	43.6	334
Fourth order Adams-Moulton (3.12)	0.76	5.5	41.4	301
Fourth order Adams-Bashforth (3.13)	1.23	9.8	74.2	568
Fourth order Milne-Simpson (3.14)	0.64	4.9	37.6	286

TABLE 2. Comparison of computational time for the different schemes (in seconds)

the second order Predictor-Corrector scheme, but the numerical error is ten times larger. However, the third order Adams-Moulton scheme (3.10) is a good compromise between accuracy and efficiency.

4.2. **Test 2 : paraxial Vlasov-Poisson model.** We apply the numerical methods presented in previous sections to the following Vlasov-Poisson system satisfied by $f(t, r, v)$, where $r \in \mathbb{R}$, $v \in \mathbb{R}$ [4, 11]

$$\left\{ \begin{array}{rcl} \dfrac{\partial f}{\partial t} + \dfrac{v}{\varepsilon}\dfrac{\partial f}{\partial r} + \left(E_f - \dfrac{r}{\varepsilon}\right)\dfrac{\partial f}{\partial v} & = & 0, \\ \dfrac{1}{r}\dfrac{\partial}{\partial r}(rE_f) & = & \displaystyle\int_{\mathbb{R}} f\,dv. \end{array} \right. \tag{4.1}$$

The electric field can be expressed explicitly as follows

$$E_f(t, r) = \frac{1}{r}\int_0^r s\,\rho(t, s)\,ds,$$

where $\rho(t, r) = \int_{\mathbb{R}} f(t, r, v)dv$, hence we will compute E_f by a simple numerical integration.

The initial condition is chosen as a Gaussian in velocity multiplied by a regularized step function in r:

$$f_0(r, v) = \frac{4}{\sqrt{2\pi\alpha}}\chi(r)\exp\left(-\frac{v^2}{2\alpha}\right), \tag{4.2}$$

with

$$\chi(r) = \frac{1}{2}\mathrm{erf}\left(\frac{r + 1.2}{0.3}\right) - \frac{1}{2}\mathrm{erf}\left(\frac{r - 1.2}{0.3}\right)$$

and $\alpha = 0.2$. The Vlasov-Poisson system (4.1) conserves mass

$$\frac{d}{dt}\int_{\mathbb{R}^2} f(t,r,v)drdv = 0,$$

and also L^p norms for $1 \leq p \leq \infty$

$$\frac{d}{dt}||f(t,r,v)||_{L^p(\mathbb{R}^2)} = 0.$$

Therefore, the evolution in time of these quantities will be observed for each scheme, especially the mass and the positivity. We will also investigate the time evolution of the kinetic energy of the Vlasov-Poisson system (4.1) :

$$\mathcal{E}(t) = \int_{\mathbb{R}^2} \frac{v^2}{2} f\, dr\, dv. \tag{4.3}$$

In the following we take the parameter $\varepsilon = 0.7$ and the computational domain is $(r,v) \in \Omega = [-4,4]^2$. On the one hand, a reference solution is presented in Figure 2 using a grid of size 800×800 and a time step of $\Delta t = 1/400$ using a fifth order space discretization for the transport equation coupled with a fourth order Runge-Rutta method for the time discretization and a fourth order method for the computation of the electric field.

On the other hand, a backward semi-Lagrangian method is applied with different type of time discretizations coupled with a fifth order Hermite interpolation. The numerical results, corresponding to the distribution function at different times, are presented in Figure 3. The grid is composed of 400×400 mesh points whereas the time step is $\Delta t = 1/100$ for the different Adams-Moulton schemes (3.9) and (3.10) and for the leap-frog scheme (2.3).

We first present the time evolution of theoretically conserved quantities like mass, L^2 norm in Figure 1. Concerning the conservation of mass, the fourth order schemes gives clearly better accuracy than the second and third order schemes. However, for the time evolution of the L^2 norm, it is not possible to distinguish the results given by the different time solvers.

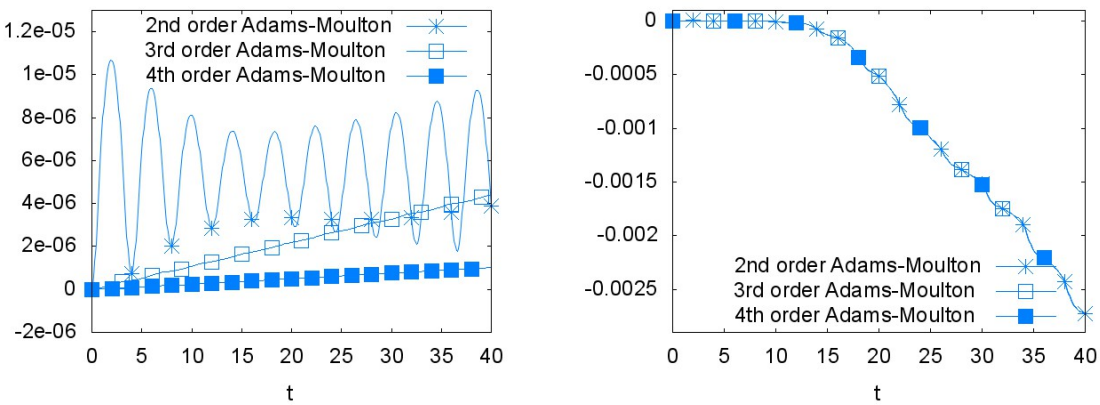

(a) relative error of mass

(b) relative error of L^2 norm

FIGURE 1. **Test 2 : paraxial Vlasov-Poisson model.** Time evolution of conserved quantities (a) mass and (b) L^2 norm for a second order Adams-Moulton scheme (3.9), a third order Adams-Moulton scheme (3.10) and a fourth order Adams-Moulton scheme (3.12) using a grid of size 400×400.

Finally, in Figures 2 and 3 we report the snapshots of the distribution function at different times $t = 5$, 15 and 50. High order Adams-Moulton schemes (3.9), (3.10) and (3.12), not shown here , give slighly the same resuts as the ones obtained with the finite difference

method. On the other hand, the leap-frog scheme generates instabilities as it has been already observed in [24].

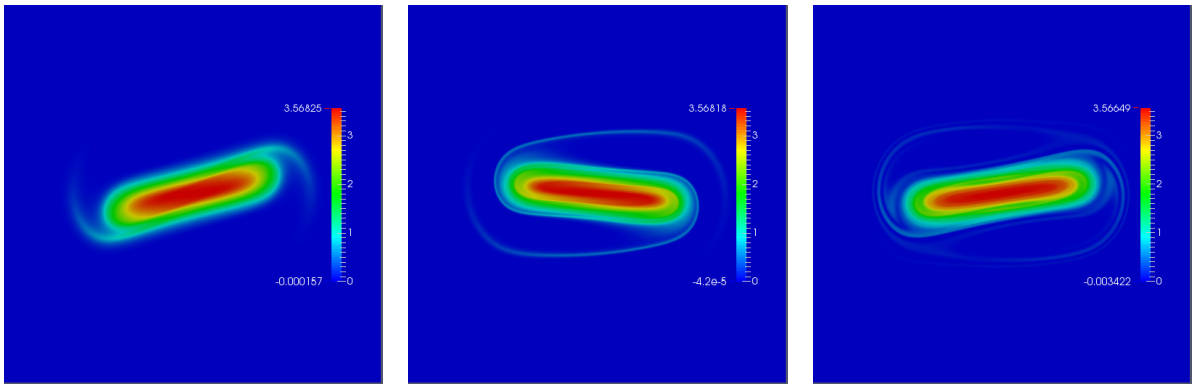

(a) $t = 5$ (b) $t = 15$ (c) $t = 50$

FIGURE 2. **Test 2 : paraxial Vlasov-Poisson model.** Reference solution computed with a high order finite difference method [24] using a grid of size 800×800.

4.3. **Test 3 : diocotron instability.** The guiding centre model [4] describes highly magnetized plasma in the poloidal plan $\mathbf{x} = (x, y) \in \mathbb{R}^2$

$$\left\{ \begin{array}{l} \dfrac{\partial \rho}{\partial t} + \mathbf{A} \cdot \nabla \rho = 0, \\ -\Delta \phi = \rho, \end{array} \right. \tag{4.4}$$

where the velocity $\mathbf{A} = (-\partial_y \phi, \partial_x \phi)$. Here we consider the model in a disk domain

$$D \;=\; \{\mathbf{x} \in \mathbb{R}^2 : \quad \|\mathbf{x}\| \leq R\}$$

and assume that the electric potential is vanishing at the boundary

$$\phi(\mathbf{x}) = 0, \quad \mathbf{x} \in \partial D. \tag{4.5}$$

Then assuming that we have zero flux at the boundary, the guiding centre model verifies the following properties :

(1) Positivity of density $0 \leq \rho(t, \mathbf{x})$.
(2) Mass conservation
$$\frac{d}{dt}\left(\int_D \rho(t, \mathbf{x}) d\mathbf{x}\right) = 0.$$
(3) L^p norm conservation, for $1 \leq p \leq \infty$
$$\frac{d}{dt}||\rho||_{L^p(D)} = 0.$$
(4) Energy conservation
$$\frac{1}{2}\frac{d}{dt}\int_D |\nabla \phi|^2(t, \mathbf{x}) d\mathbf{x} \;=\; \frac{d}{dt}\int_D \rho(t, \mathbf{x})\, \phi(t, \mathbf{x}) d\mathbf{x} \;=\; 0.$$

For this test we consider the diocotron instability for an annular electron layer. The initial data is given by

$$\rho_0(\mathbf{x}) = \left\{ \begin{array}{ll} (1 + \varepsilon \cos(\ell\theta)) \exp\left(-4(r - 6.5)^2\right), & \text{if } r^- \leq \|\mathbf{x}\| \leq r^+, \\ 0, & \text{otherwise}, \end{array} \right.$$

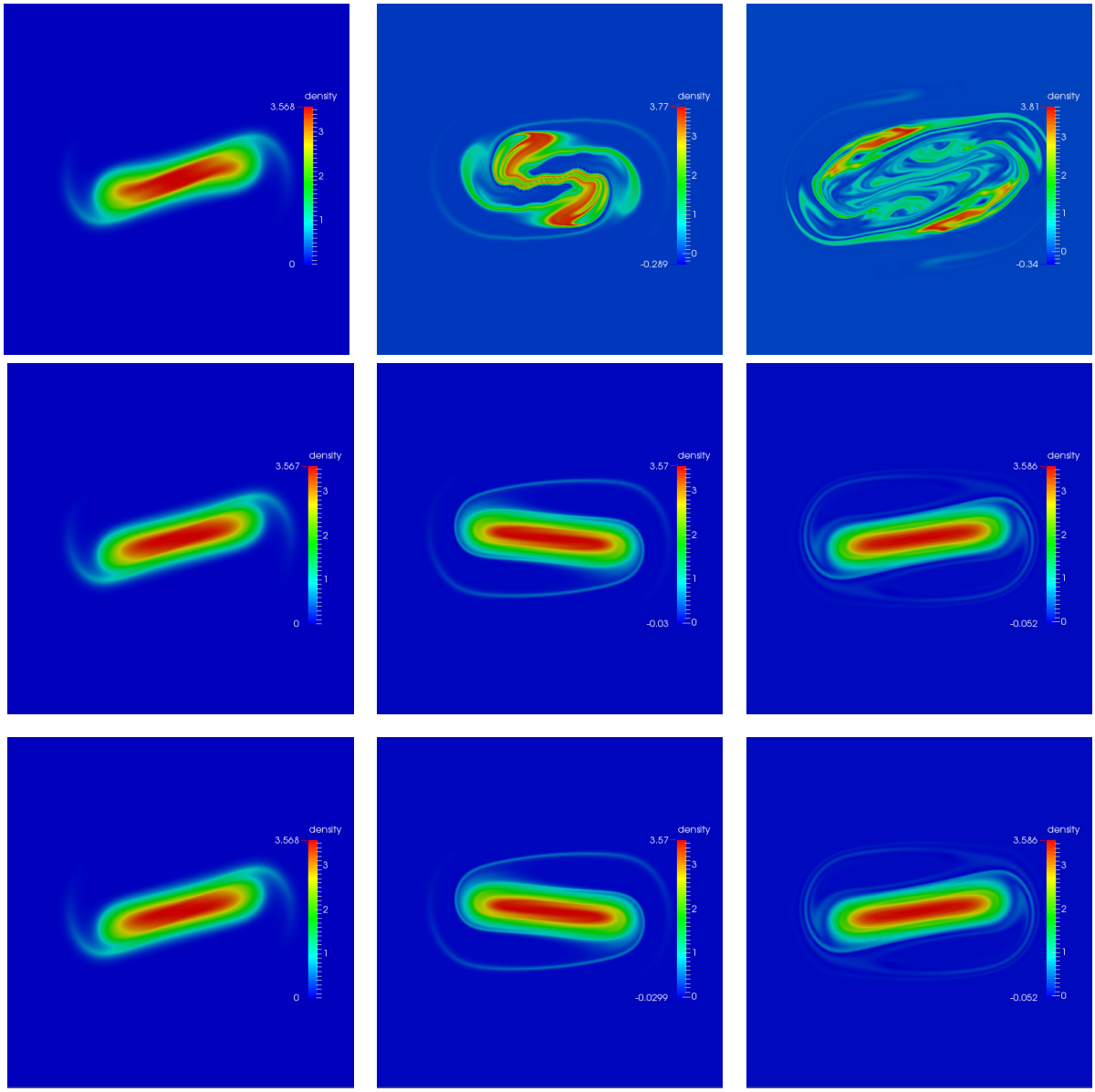

(a) $t = 5$ (b) $t = 15$ (c) $t = 50$

FIGURE 3. **Test 2 : paraxial Vlasov-Poisson model.** Numerical solution computed with (top) a leap-frog scheme (2.3) (middle) a second order Adams-Moulton scheme (3.9) and (bottom) a third order Adams-Moulton scheme (3.10) using a grid of size 400×400.

where ε is a small parameter, $\theta = \text{atan}(y/x)$. In the following tests, we take $\varepsilon = 0.001$, $r^- = 5$, $r^+ = 8$, $\ell = 7$, furthermore $\Delta t = 0.05$ and $h = \Delta x = \Delta y = 24/1000$.

We compare the results obtained with the backward semi-Lagrangian method presented in Figure 6, to the reference results obtained in Figure 5. Here, the different schemes give very similar results. The slight differences can be seen looking at Figure 4. Indeed mass, L^2 norm and energy conservation are much better with the third order Adams-Moulton scheme than with the second order. Oddly here the results with the Adams-Moulton scheme of order four are not better than those obtained with the third order. Regarding the minimum of

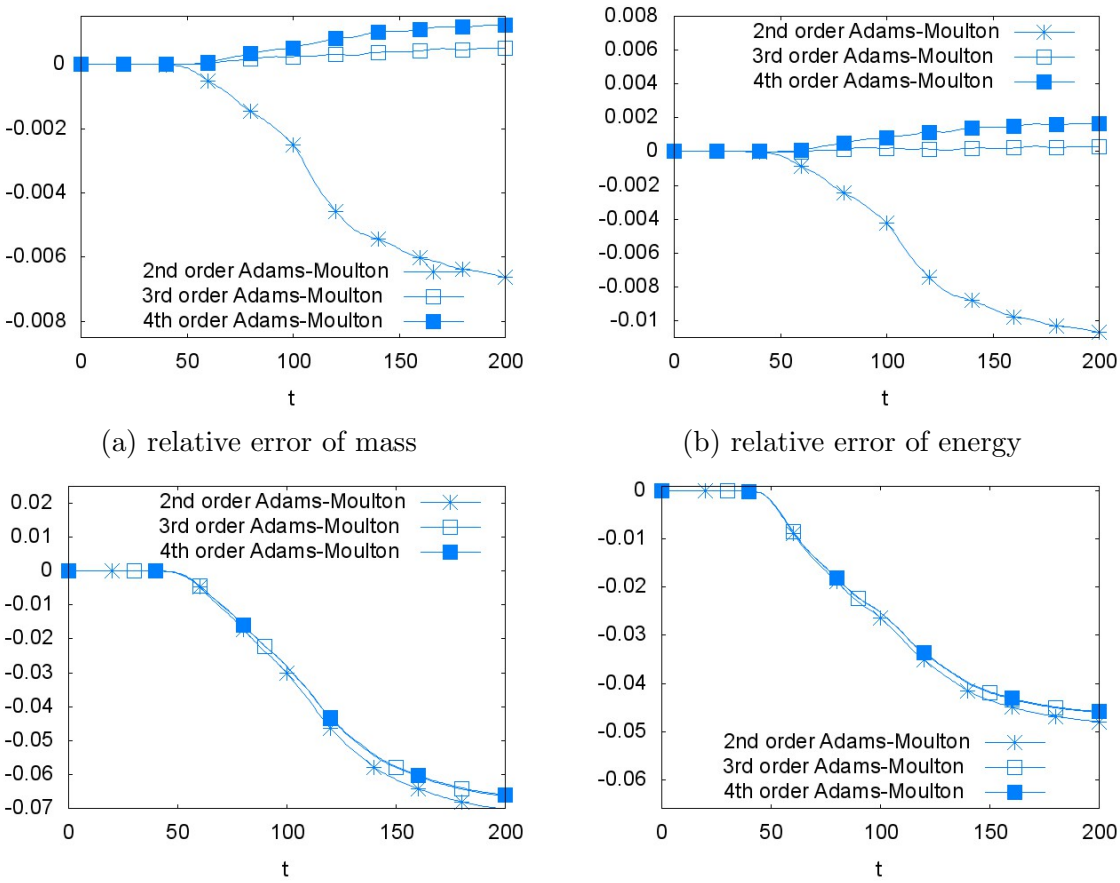

(a) relative error of mass

(b) relative error of energy

(c) relative error of L^2 norm

(d) relative error of L^4 norm

FIGURE 4. **Test 3 : diocotron instability.** Time evolution of conserved quantities (a) mass and (b) energy (c) L^2 norm and (d) L^4 norm for a second order Adams-Moulton scheme (3.9), a third order Adams-Moulton scheme (3.10) and a fourth order Adams-Moulton scheme (3.12) using a grid of size 1000×1000.

the distribution function there are no significant differences. Hence, as it has been observed before, the third order Adams-Moulton scheme (3.10) is a good compromise here between accuracy and efficiency.

4.4. **Test 4 : Kelvin-Helmoltz instability in a rectangle.** We still consider the guiding centre model but now the computational domain is a rectangle with periodic boundary conditions in the x direction and Dirichlet in the y direction[21]. The initial distribution function is

$$\rho_0(\mathbf{x}) \;=\; \sin(y)\;(1 \;+\; 0.005\;\cos(k_x x)), \quad \mathbf{x} = (x, y) \in (0, Lx) \times (0, 2\pi),$$

with $k_x = 2\pi/L_x$. We choose $L_x = 10$ in such a way that the solution will generate an instability [21].

For this test, we choose to run the code on very fine meshes 2048×2048 points and the Poisson equation with periodic boundary conditions in x and homogeneous Dirichlet condition in y is dicretized using a classical fast Fourier transform giving high order accuracy. Concerning the time discretization we still apply the second (3.9), third (3.10) and fourth (3.12) order Adams-Moulton schemes In Figure 7, we present the time evolution of macroscopic quantities

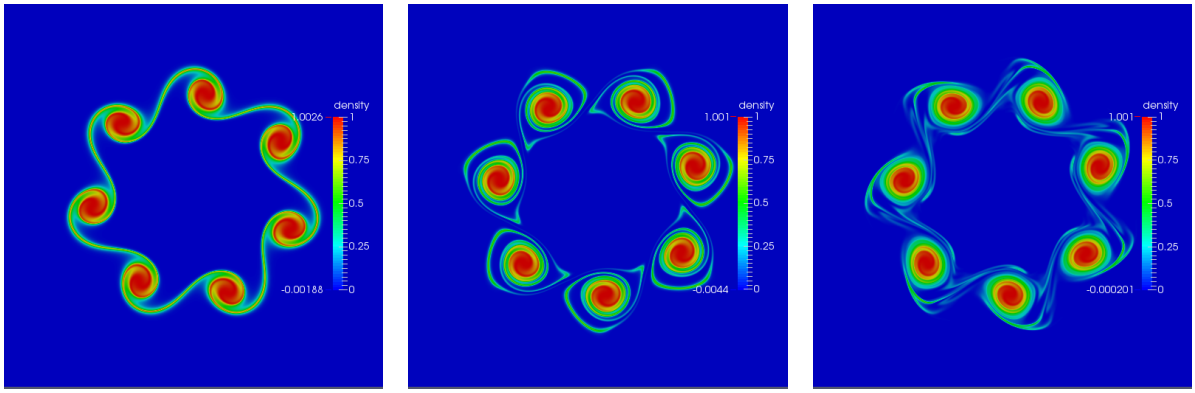

(a) $t = 50$ (b) $t = 70$ (c) $t = 100$

FIGURE 5. **Test 3 : diocotron instability.** Reference solution computed with a high order finite difference method [24] using a grid of size 1000×1000.

such as mass, energy and L^p norms. Once more the third and fourth order schemes allow to improve the conservation of mass and energy, but cannot avoid the numerical dissipation of L^p norms.

4.5. **Test 5 : shear flow for 2D Euler equations.** We consider the 2D incompressible Euler system in the vorticity formulation with a shear flow:

$$\begin{cases} \dfrac{\partial \rho}{\partial t} + \mathbf{U} \cdot \nabla \rho = 0, \\ -\Delta \phi = \rho, \end{cases} \tag{4.6}$$

where the velocity $\mathbf{U} = (-\partial_y \phi, \partial_x \phi)$. Here $\mathbf{x} = (x, y) \in \mathbb{T} \times (0, 2\pi)$, with periodic boundary conditions in x and homogeneous Dirichlet like boundary condition in $y = 0$ and 2π, and ϕ denotes the streamfunction which verifies homogeneous Dirichlet boundary condition.

In this work, we are interested in the long time simulation of (4.6) for small initial perturbations of a stable steady state. Recently, J. Bedrossian and N. Masmoudi [2] proved that for a smooth and small enough initial perturbation of amplitude ϵ, the solution to (4.6) converges to a new equalibrium and that the velocity field $\mathbf{U} = (U_x, U_y)$ satisfies when t goes to infinity

$$\|U_y\|_{L^2} \leq \frac{C\epsilon}{t^2}$$

and

$$\|U_x - < U_x > \|_{L^2} \leq \frac{C\epsilon}{t},$$

where $< U_x >$ denotes the local average of U_x with respect to the x variable. Here we consider the equilibrium $\rho_{eq} = \sin(y)$ and introduce a small perturbation $\delta\rho = \varepsilon \cos(kx) \sin(y)$. In Figure 8, we present the time evolution of these quantities with respect to time obtained with the third order Adams-Moulton scheme. The numerical solution follow the correct long time behavior and the convergence to equilibrium is given with the expected rate of convergence : $1/t$ for the quantity $\|U_x - < U_x > \|_{L^2}$ whereas the quantity $\|U_y\|_{L^2}$ is of order $1/t^2$. Finally in Figure 9, we present the snapshots of the vorticity $\rho - \rho_{eq}$ for different times $t = 20$, 40 and 60 and observed that due to periodic boundary conditions oscillations in the y component appear and generate higher and higher frequencies.

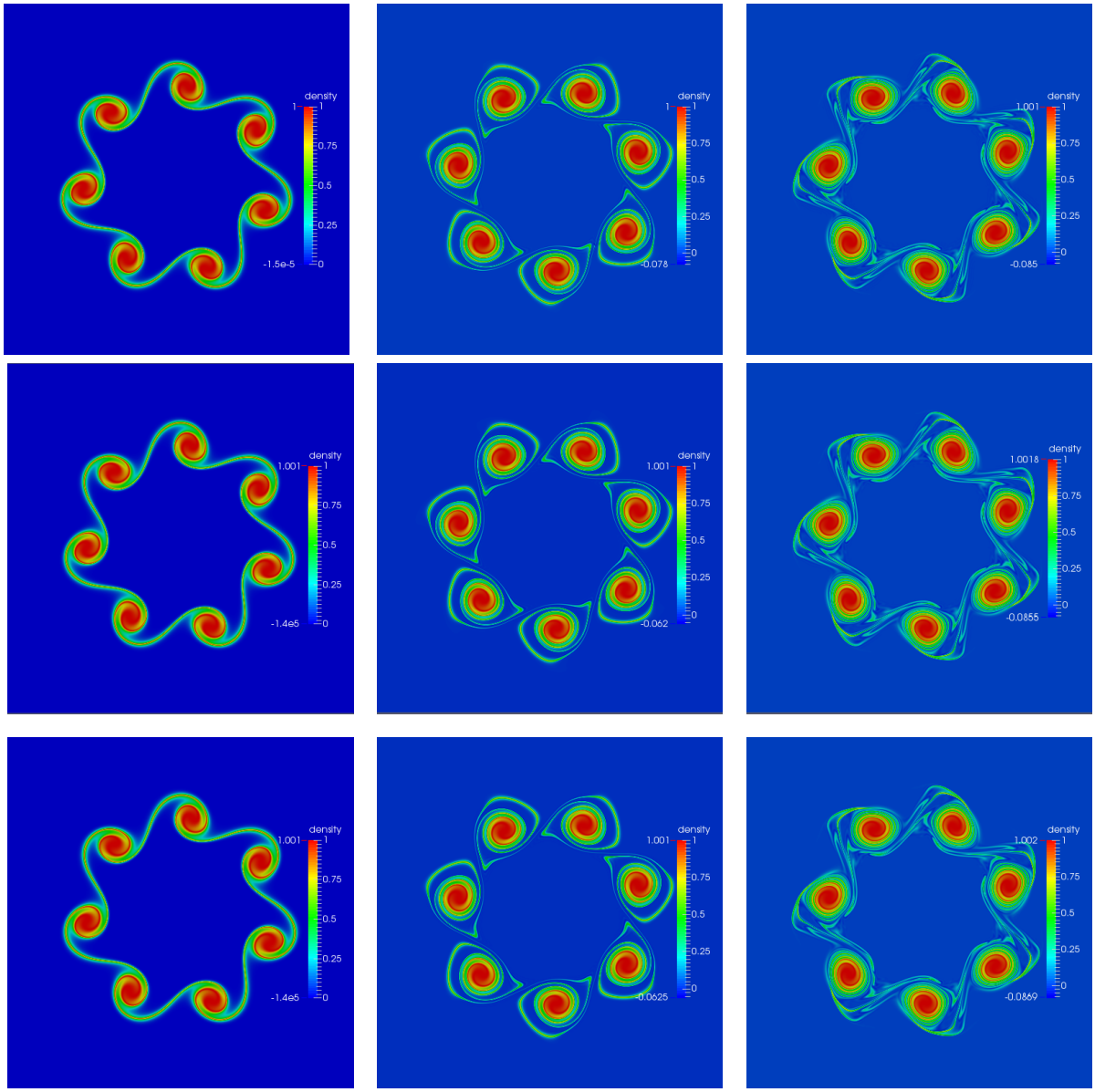

(a) $t = 50$ (b) $t = 70$ (c) $t = 100$

FIGURE 6. **Test 3 : Diocotron instability.** Numerical solution computed with (top) a leap-frog scheme (2.3) (middle) a second order Adams-Moulton scheme (3.9) and (bottom) a third order Adams-Moulton scheme (3.10) using a grid of size 1000×1000.

5. Conclusion and perspective

In this paper we have developed and compared several time discretization techniques for the backward semi-Lagrangian method. We obverve that when the spatial mesh is fine enough and the spatial discretization error negligeable, the high order Adams-Moulton scheme brought better results than the classical schemes. In particular, the results reveal a major improvements in terms of mass and energy conservations. Hence the application of a higher order

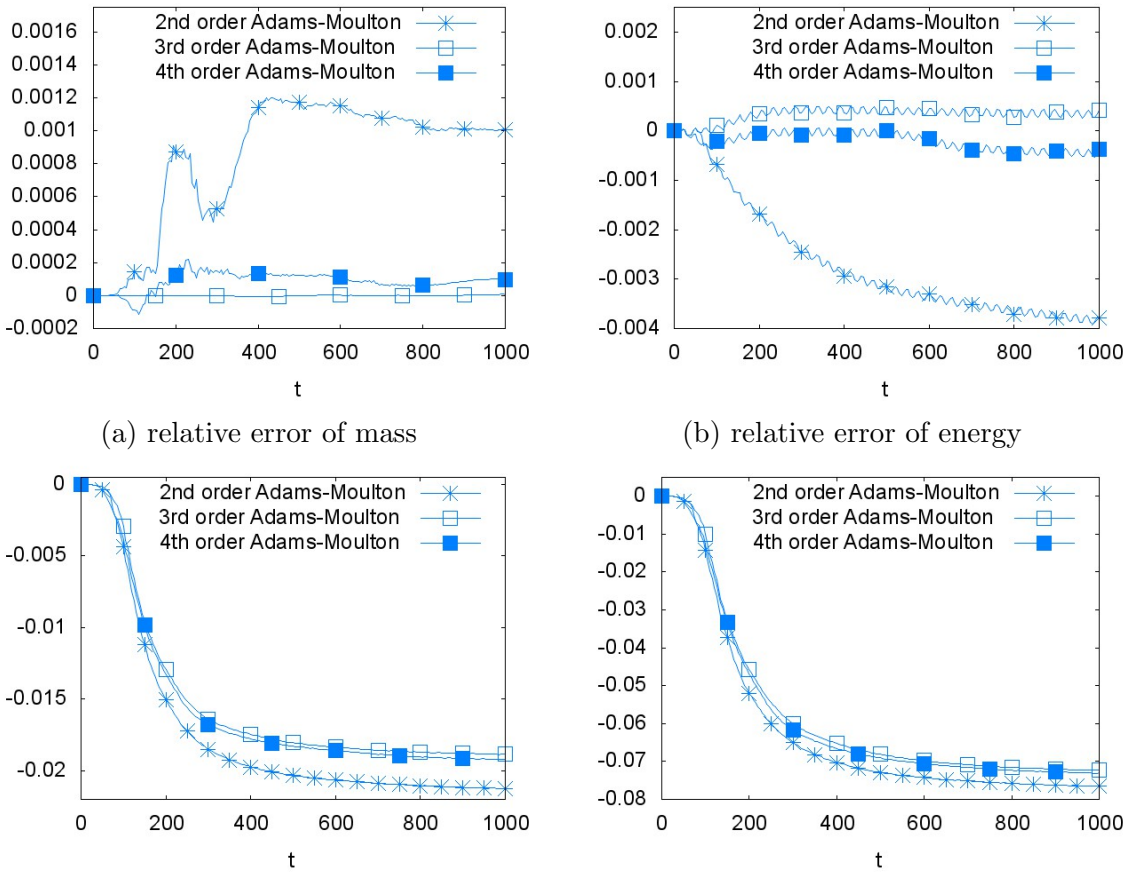

(a) relative error of mass

(b) relative error of energy

(c) relative error of L^2 norm

(d) relative error of L^4 norm

FIGURE 7. **Test 4 : Kelvin-Helmoltz instability in a rectangle.** Time evolution of conserved quantities (a) mass, (b) energy, (c) L^2 norm and (d) L^4 norm for a second order Adams-Moulton scheme (3.9), a third order Adams-Moulton scheme (3.10) and a fourth order Adams-Moulton scheme (3.12) using a grid of size 2048×2048.

schemes is justified, although in our numerical simulations four order schemes brought few improvements compared to the third order discretization. Finally, the third order Adams-Moulton scheme (3.10) is computationally interesting, robust and accurate for various numerical tests.

REFERENCES

[1] B. AFEYAN, F. CASAS, N. CROUSEILLES, A. DODHY, E. FAOU, M. MEHRENBERGER, E. SONNENDRUCKER, Simulations of Kinetic Electrostatic Electron Nonlinear (KEEN) Waves with Two-Grid, Variable Velocity Resolution and High-Order Time-Splitting, EPJD, topical issue of Vlasovia (2013).

[2] J. BEDROSSIAN, N. MASMOUDI, Asymptotic stability for the couette flow in the 2D Euler equations, arXiv: 1309.2035v1, (2013).

[3] N. CROUSEILLES, M. MEHRENBERGER AND E. SONNENDRUCKER, Conservative semi-Lagrangian schemes for Vlasov equations, *Journal of Computational Physics*, **229**, (2010), pp. 1927–1953.

[4] N. CROUSEILLES, M. LEMOU AND F. MÉHATS, Asymptotic preserving schemes for highly oscillatory VlasovPoisson equations, *Journal of Computational Physics*, **248**, (2013), pp. 287–308.

[5] B. A. DE DIOS, J. A. CARRILLO AND C.W. SHU, Discontinuous Galerkin methods for the multidimensional Vlasov-Poisson problem, *Mathematical Models and Methods in Applied Sciences*, **22**, (2012).

[6] M. R. FEIX, P. BERTRAND AND A. GHIZZO, Eulerian codes for the Vlasov equation *Series on Advances in Mathematics for Applied Sciences* 22, *Kinetic Theory and Computing*, (1994), pp. 45

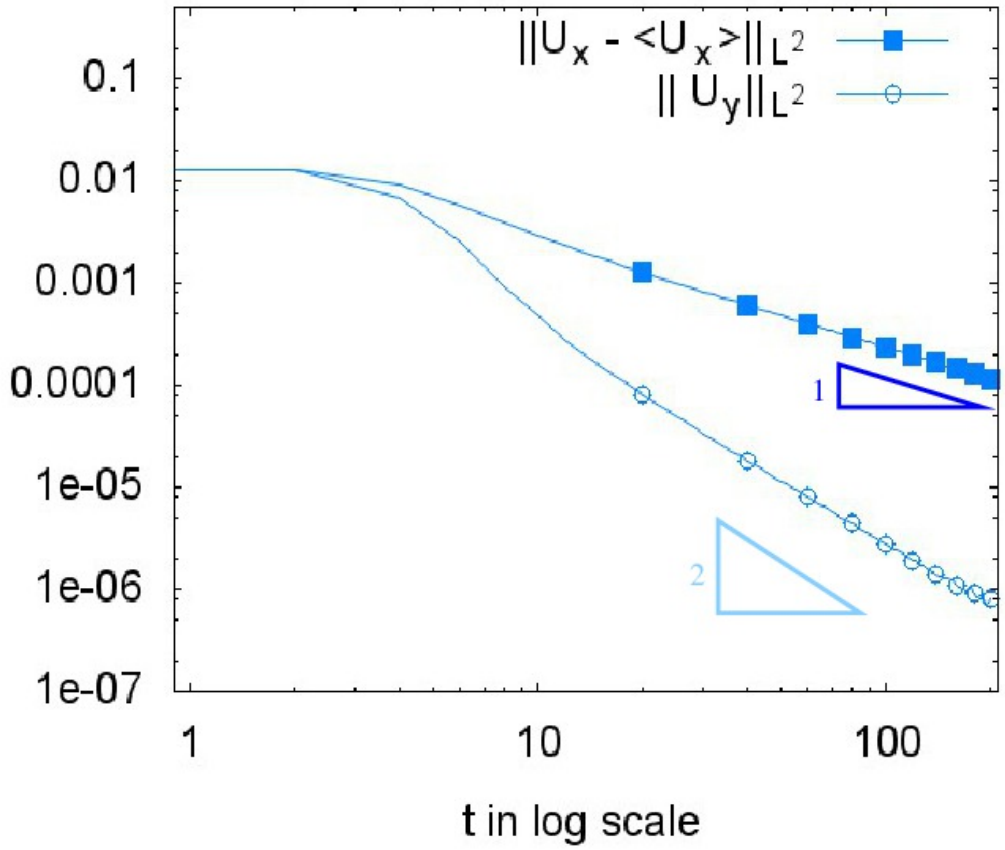

FIGURE 8. **Test 5 : shear flow for 2D Euler equations.** Time evolution of $\|U_x - < U_x > \|_{L^2}$ and $\|U_y\|_{L^2}$using the third order Adams-Moulton scheme (3.10) with a grid of size 256×4096.

[7] F. FILBET, Convergence of a Finite Volume Scheme for the One Dimensional Vlasov-Poisson System, *SIAM J. Numer. Analysis*, **39**, (2001), pp. 1146–1169.

[8] F. FILBET, R. DUCLOUS AND B. DUBROCA, Analysis of a high order finite volume scheme for the Vlasov-Poisson system, *DCDS-S*, **5** (2012), pp. 283–305.

[9] F. FILBET, E. SONNENDRÜCKER, P. BERTRAND, Conservative numerical schemes for the Vlasov equation, *Journal of Computational Physics*, **172**, (2001), pp. 166–187.

[10] F. FILBET, E. SONNENDRÜCKER, Comparison of Eulerian Vlasov solvers, *Computer Physics Communications*, **150** (2003), pp. 247–266.

[11] F. FILBET, E. SONNENDRÜCKER, Modeling and numerical simulation of space charge dominated beams in the paraxial approximation, *Mathematical Models and Methods in the Applied Sciences*, **16**, (2006), pp. 763–791.

[12] A. GHIZZO, P. BERTRAND, M. SHOUCRI, T. W. JOHNSTON, E. FILJAKOW AND M. R. FEIX, A Vlasov code for the numerical simulation of stimulated Raman scattering *J. Comput. Phys.* **90**, (1990), pp 431.

[13] V. GRANDGIRARD, M. BRUNETTI, P. BERTRAND, N. BESSE, X. GARBET, P. GHENDRIH, G. MANFREDI, Y. SARAZIN, O. SAUTER, E. SONNENDRÜCKER, J. VACLAVIK AND L. VILLARD, A drift-kinetic semi-Lagrangian 4D code for ion turbulence simulation, *Journal of Computational Physics*, **217**, (2006), pp. 395–423.

[14] V. GRANDGIRARD, Y. SARAZIN, X. GARBET, G. DIF-PRADALIER, P. GHENDRIH, N. CROUSEILLES, G. LATU, E. SONNENDRÜCKER AND N. BESSE, Computing ITG turbulence with a full-f semi-Lagrangian code, *Communications in Nonlinear Science and Numerical Simulation*, **13**, (2008), pp. 81–87.

[15] W. GUO AND J. - M. QIU, Hybrid semi-Lagrangian finite element-finite difference methods for the Vlasov equation, *Journal of Computational Physics*, **234**, (2013), pp. 108–132.

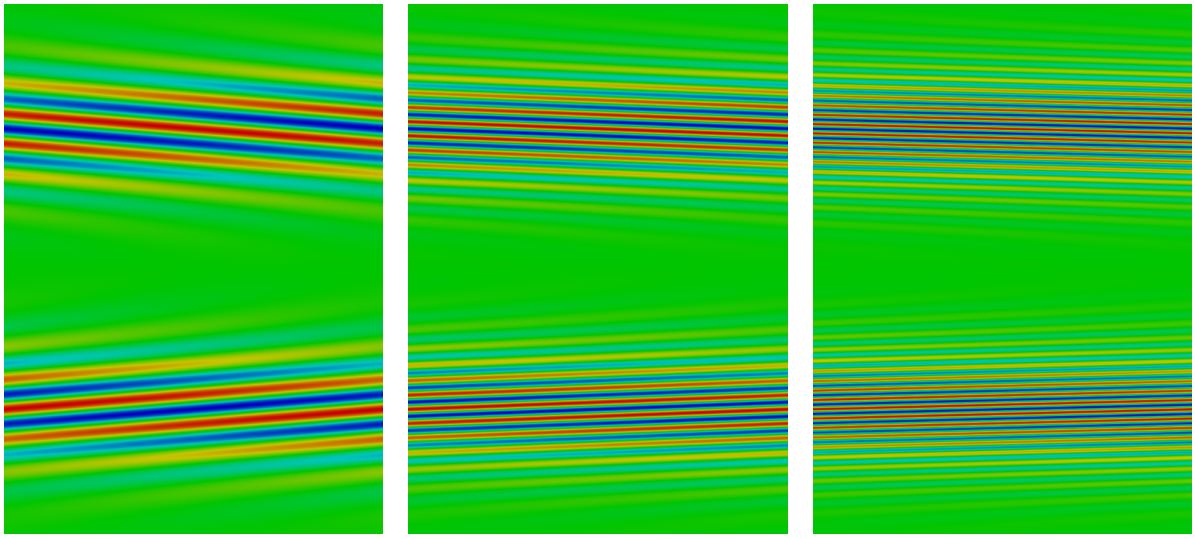

(a) $t = 20$ (b) $t = 40$ (c) $t = 60$

FIGURE 9. **Test 5 : shear flow for 2D Euler equations.** Snapshots of the vorticity $\rho - \rho_{eq}$ for different times $t = 20$, 40 and 60 using the third order Adams-Moulton scheme (3.10) with a grid of size 256×4096.

[16] E. HAIRER, S.P. NRSETT AND G. WANNER, Solving ordinary differential equations. I. Nonstiff problems. Second edition. Springer Series in Computational Mathematics, 8. Springer-Verlag, Berlin, 1993. xvi+528 pp.

[17] R. E. HEATH, I. M. GAMBA, P.J. MORRISON AND C. MICHLER, A discontinuous Galerkin method for the Vlasov-Poisson system, *Journal of Computational Physics*, **231**, (2012), pp. 1140–1174.

[18] J. M. QIU AND C. -W. SHU, Positivity preserving semi-Lagrangian discontinuous Galerkin formulation: theoretical analysis and application to the Vlasov-Poisson system, *Journal of Computational Physics*, **230** (2011), pp. 8386–8409.

[19] E. SHIKIN AND A. PLIS, Handbook on splines for the user, *CRC Press*, (1995).

[20] M. SHOUCRI AND G. KNORR, Numerical integration of the Vlasov equation *J. Comput. Physics*, **14**, (1974), pp. 84–92.

[21] E. SONNENDRÜCKER, J. ROCHE, P. BERTRAND AND A. GHIZZO, The Semi-Lagrangian Method for the Numerical Resolution of Vlasov Equations. *J. Comput. Phys.* , **149**, (1998), pp. 201–220.

[22] T. NAKAMURA AND T. YABE, Cubic interpolated propagation scheme for solving the hyper-dimensional Vlasov-Poisson equation in phase space, *Comput. Phys. Communications*, **120**, (1999), pp. 122–154.

[23] T. UMEDA, Y. NARIYUKI, D. KARIYA, A non-oscillatory and conservative semi-Lagrangian scheme with fourth-degree polynomial interpolation for solving the Vlasov equation, *Computer Physics Communications*, **183**, (2012), pp. 1094–1100.

[24] C. YANG, F. FILBET, Conservative and non-conservative methods based on Hermite weighted essentially non-oscillatory reconstruction for Vlasov equations, *J. Comput. Physics,* **279** , (2014), pp. 18-36.

[25] H.YOSHIDA, Construction of higher order symplectic integrators, *Physics Letters A*, **150**, (1990).